J Nanopart Res (2023) 25:21
https://doi.org/10.1007/s11051-022-05666-2

RESEARCH PAPER

Core-shell structured MCM-48-type silica-polymer hybrid material synthesis and characterization

Shewaye Yismaw · Marianne Wenzel · Ahmed Gamal Attallah · Radosław Zaleski · Jörg Matysik · David Poppitz · Roger Gläser · Stefan G. Ebbinghaus · Dirk Enke

Received: 14 May 2022 / Accepted: 29 December 2022 / Published online: 11 January 2023

Abstract In the current study, a core-shell structured material of MCM-48-type mesoporous silica nanoparticles (MSNs) and cross-linked poly(N-isopropylacrylamide) homopolymer and its copolymer with methacrylic acid was synthesized. The polymer was preferentially grafted on the outer surface of silane linker-functionalized MSNs based on free radical polymerization. The successful chemical grafting of the polymer on the silica surface was confirmed by FTIR, NMR, TG, and elemental analyses. The polymer contents of the hybrid particles vary from 18 to 40 % as determined by thermogravimetric and elemental analyses. The polymer content was tailored by varying different reaction parameters including monomer concentration, linker content/type, and reaction time. Well-defined uniform core-shell structured spherical particles with an average particle size of 367 ± 25 nm and shell thickness of 29 ± 8 nm were observed in TEM analysis. According to XRD and nitrogen physisorption studies, the ordered mesopore structure of the core MCM-48-type MSNs was maintained after an extended polymer grafting process and surface coverage with a high content of polymer. No significant pore blockage was observed in porosimetry analysis. More than 75% of specific surface area, 68% of total pore volume, and the mean mesopore diameter were retained after successful grating of polymer on the outer silica surface. The pore volume thus can provide enough space to encapsulate high

Supplementary Information The online version contains supplementary material available at https://doi.org/10.1007/s11051-022-05666-2.

S. Yismaw · D. Poppitz · R. Gläser · D. Enke (✉)
Institute of Chemical Technology, Universität Leipzig, Linnéstraße 3, 04103 Leipzig, Germany
e-mail: dirk.enke@uni-leipzig.de

S. Yismaw (✉)
Department of Chemistry, University of Gondar, P.O. Box 196, Gondar, Ethiopia
e-mail: shewayeyismaw@yahoo.com

M. Wenzel · J. Matysik
Institute of Analytical Chemistry, Universität Leipzig, Linnéstraße 3, 04103 Leipzig, Germany

A. G. Attallah
Helmholtz-Zentrum Dresden-Rossendorf, Bautzner Landstraße 400, 01328 Dresden, Germany

A. G. Attallah
Department of Physics, Minia University, 61519, Minia, Egypt

R. Zaleski
Institute of Physics, Maria Curie-Sklodowska University, Pl. M. Curie-Sklodowskiej 1, 20-031 Lublin, Poland

S. G. Ebbinghaus
Institute of Chemistry, Martin-Luther-Universität Halle-Wittenberg, Kurt-Mothes-Straße 2, 06120 Halle (Saale), Germany

contents of cargo molecules for applications. The narrow pore width distribution of the main mesopores of silica determined by PALS analysis corresponds to the N_2 sorption analysis and further confirms the uniformity of the mesopores.

Keywords MCM-48-type mesoporous silica nanoparticles · Hybrid material · Core-shell structure · Polymer · Grafting · Synthesis

Introduction

Mesoporous silica nanoparticles (MSNs) on the basis of MCM-41, MCM-48, and SBA-15 materials, which are characterized by high specific surface area, large pore volume, uniform particle width, tunable surface chemistries, and good thermal stability, are of great research interest as "containers" for drug delivery systems [1]. To tailor their application, these particles mostly require appropriate surface modification. Hence, hybrid materials of MSNs and stimuli-responsive polymers can provide unique properties offered by both the inorganic and organic components (e.g., flexibility, ductility, and chemical functionality). Therefore, to enhance the properties of either of the components, the polymeric units are commonly grafted chemically on the surface of MSNs supports via grafting to, grafting from, or grafting through approaches [2]. Poly(*N*-isopropylacrylamide) (PNIPAM) is a well-known non-toxic and water-soluble polymer used in diverse applications, for instance, in gas adsorption [3], waste water treatment [4], and drug delivery [5]. Frequently, conventional polymer-based applications usually suffer from problems such as poor mechanical stability and relatively low loading capacity [6]. Hence, the synthesis of different types of silica and stimuli-responsive polymer/copolymer composite materials is studied broadly for their biomedical applications [7–10].

MCM-48-type MSNs with three-dimensional interconnected pore network offer more efficient diffusion pathways and adsorption sites compared to one-dimensional hexagonal MCM-41 and SBA-15 structured silica, which are the most widely explored materials for biomedical applications [11]. Thus, MCM-48 types of modified mesoporous silica nanoparticles can be used as a good platform for various applications, but the surface modification and detail characterizations are not extensively studied until now. He et al. prepared a hybrid of MCM-48-polystyrene nanoparticles through in situ free radical polymerization and demonstrated a significant improvement in the mechanical properties of the polymer [12]. Kalbasi and Mosaddegh studied nanohybrid based on poly(4-vinylpyridine) and MCM-48 silica and effectively employed the material as a novel heterogeneous basic catalyst [13]. Recently, Meléndez-Ortiz et al. prepared MCM-48 mesoporous silica filled with polyacrylamide using an azo-type initiator and evaluated the effect of various reaction parameters to determine the optimal grafting conditions [14]. The hybrid nanoparticles showed high drug loading capacity and sustained delivery behavior.

Though, there is no prior detailed investigation focused on the synthesis and physicochemical characterization of MCM-48-type silica-stimuli-responsive polymer core-shell structured materials. In this study, we present the chemical grafting of a cross-linked PNIPAM-based polymer preferentially on the outer surface of MCM-48 structure MSNs as a core-shell structure, keeping the inner pore surface of the particle with optimal textural properties for sufficient loading of guest molecules inside the porous particles. The synthesized hybrid particles possess several potential applications in temperature-triggered systems. Besides, the effects of various reaction parameters (monomer/co-monomer concentration, silane linker content and its type in terms of linker chain length, and reaction time) on the amount of the final polymer grafted on the surface of silica were studied by TG and CHN elemental analyses. The controlled quantitative grafting technique presented in this work can be applied for the grafting of PNIPAM and its copolymers on nanoparticles with relatively intact morphology and mesopore structures. To the best of our knowledge, this is the first deep systematic investigation on the structural and morphological features and textural parameters of the resultant MCM-48-based hybrid particles (MS-PNM$_{x\%}$, Fig. 1) using various analytical techniques. The designed well-defined inorganic silica-organic polymer (MS-PNM$_{x\%}$) core-shell structure nanoparticles with optimal textural properties will be used for the purpose of controlled drug delivery system in a subsequent study.

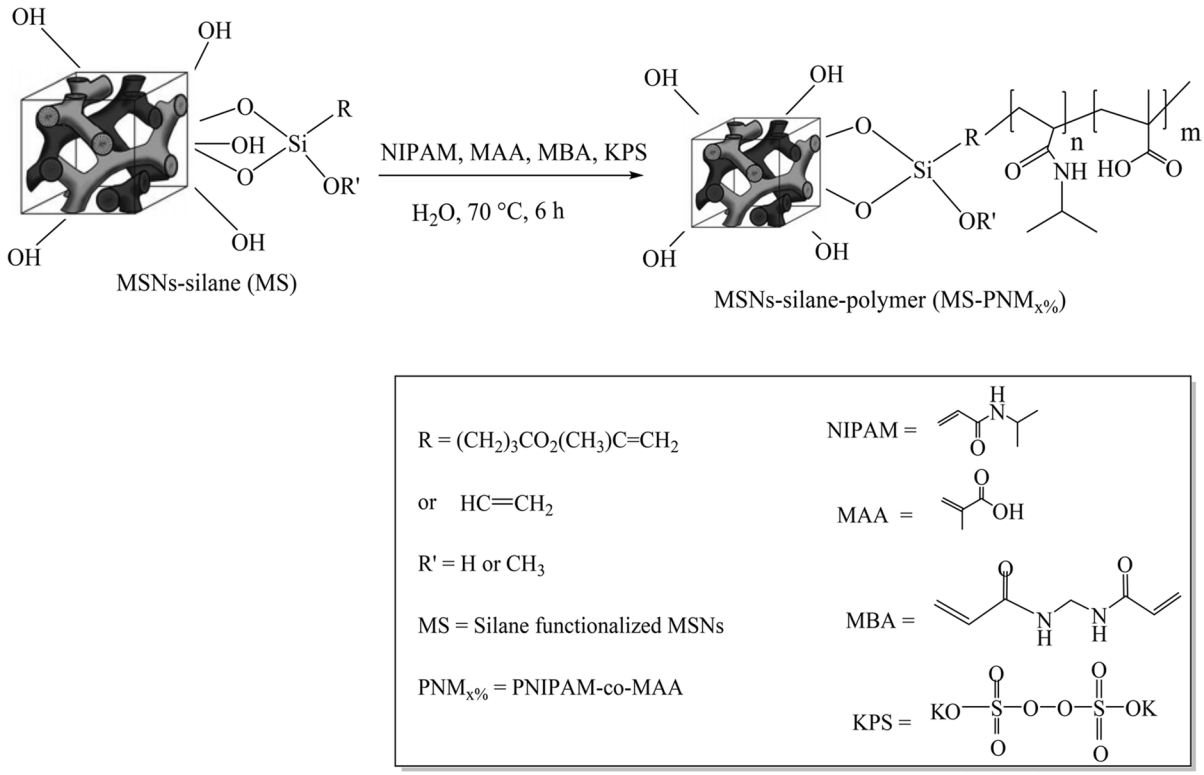

Fig. 1 Synthetic scheme for the preparation of silane-functionalized MCM-48-type MSNs-polymer hybrid nanoparticles

Experimental

Chemicals

N-Isopropylacrylamide (NIPAM, 99 %) and potassium persulfate (KPS, 99%) were purchased from Acros-organics (Geel, Belgium). Methacrylic acid (MAA, 99%) was received from Merck (Darmstadt, Germany). N,N′-Methylenebisacrylamide (MBA, 99%) was purchased from Sigma Aldrich (Steinheim, Germany). 3-Methacryloxypropyltrimethoxy-silane (MPS, 98%) and vinyltrimethoxy-silane (VTMS, 98%) were received from Alfa Aesar (Karlsruhe, Germany). All chemicals and solvents used for the synthesis were of high purity and used as received without further purification. Deionized water was used in all syntheses.

Synthesis of polymer-coated MCM-48 silica hybrid materials

MCM-48 structured MSNs with average particle size of 295 nm and their outer surface functionalization with organosilanes were prepared by adapting the synthesis procedure described by Yismaw et al. [15, 16]. The preferential outer surface functionalization of the MCM-48 nanoparticles with the linker organosilane molecules was addressed by either post-synthetic route for the synthesized particles containing the template still inside the pore channels or by co-condensation route via late addition of the silane precursors into the synthesis batch containing a fully grown silica [16]. The MSNs containing active functional groups were used as a core for the subsequent polymer grafting process on the outer surface. The content of silanes on the MSNs surface following selective outer surface functionalization using MPS was calculated based on the external surface area of the as-synthesized material. The observed values were 16 and 29 molecules nm^{-2} for samples prepared via post synthesis route using ethanol (MM1E) and toluene (MM1T) as a solvent, respectively. In contrast, the sample prepared via condensation route (MM-Co_{35}) contained 40 molecules nm^{-2} [16]. Herein, for comparison purpose of the surface

functionalization with long-chain length acryloxy linker groups of MPS, MSNs functionalized by VTMS with relatively short-chain length vinyl linker groups are also considered (Table 1). The experimental procedure for VTMS silica outer surface functionalization (MV1T) was similar to the reported MPS postsynthetic functionalization route [16].

The silica-polymer hybrid particles were synthesized via grafting through/from free radical polymerization approaches. Hence, the MSNs previously functionalized using MPS or VTMS containing different contents of active vinyl functional groups (denoted as MS in Fig. 1) were used as a core for free radical polymerization progression. NIPAM, MAA, MBA, and KPS were used as monomer, co-monomer, cross-linker, and initiator, respectively, for the polymerization reaction. Briefly, a selected silane-modified MSNs sample (MS) (1 g) was dispersed in 50 ml deionized water. Since MPS-functionalized particles are fluffy and show poor wetting by water, a small amount of absolute ethanol (10 ml) was added for complete dispersion. A transparent solution of NIPAM (0.9 g, 7.95 mmol), MAA (30 µl, 0.34 mmol), and MBA (0.014 mg, 0.10 mmol) was prepared in 50 ml deionized water in a separate flask (Table S1) and transferred into the above silica dispersion. The monomer, co-monomer, and cross-linker amounts were varied individually (Table S1). The cross-linkers (MBA) with two active sites show a higher reaction rate compared to the NIPAM monomer [17]. Hence, a very low concentration of this component was used to overcome its heterogeneous distribution in the copolymer network. The mixed solution was directly bubbled with nitrogen flow for 30 min to remove water-solubilized residual oxygen. The mixture was heated in a three-neck bottom flask equipped with a condenser to 70 °C in an oil bath under mechanical stirring at 300 rpm for 1 h in a nitrogen atmosphere. Then, a solution of KPS prepared in a separate vial (30 mg ml^{-1}, 0.11 mmol) was rapidly added under nitrogen flow. The free radical polymerization reaction (grafting through) onto the surface of silica particles functionalized with polymerizable vinyl groups [18] was left to further proceed for 6 h at 70 °C under nitrogen protection. Alternatively, a solution of KPS was added into the degassed dispersion of silane-functionalized silica and left for 1 h at 70 °C where the free radicals are formed on the surfaces of silica particles. Then, the transparent monomeric solution was degassed and transferred into the dispersed silica containing the initiator and the reaction continued for 6 h. For the graft polymerization process, the monomer can be initiated on the solid particles (grafting from) via a redox surface-initiating system at the interface between the particles and solution. However, there were no significant differences between the samples prepared via these two approaches (apart from minimal variations in the final polymer grafting amount). Therefore, the grafting through approach was implemented throughout this work. Finally, the hybrid nanoparticles were collected by centrifugation and washed repeatedly with water and ethanol under shaking to remove unreacted components as well as non-grafted polymer chains. The synthesized hybrid materials were dried at 50 °C for 48 h under vacuum and are named as MS-$PNM_{x\%}$ (Fig. 1) which represents MM1E-$PNM_{x\%}$, MM1T-$PNM_{x\%}$, MV1T-$PNM_{x\%}$, or MM-Co_{35}-$PNM_{x\%}$ throughout the "Results and discussion" section. $X_{\%}$

Table 1 Nomenclature and synthetic conditions of silane-functionalized MCM-48 silica samples with the corresponding silane grafting density considered for further polymer grafting process

Sample	Functionalization route	Silane type	Solvent used	Functional group	ΔC [wt.%][a]	X_{EA} [molecules nm^{-2}][b]
MM1E	Postsynthetic	MPS	Ethanol	Acryloxy	4.2	16
MM1T	Postsynthetic	MPS	Toluene	Acryloxy	7.2	29
MV1T	Postsynthetic	VTMS	Toluene	Vinyl	3.5	52
MM-Co_{35}	Co-condensation	MPS	---------	Acryloxy	9.3	40

[a]Actual carbon content (ΔC) of silane-functionalized silica estimated from elemental analysis and [b]grafting density of silanes (X_{EA}) calculated on basis of the external surface area (S_{ex}) [16]

refers to the mol% of the co-monomer MAA applied during the polymerization process.

Characterization

Fourier transform infrared spectroscopy (FTIR) measurements were performed with a vector 22 ATR-FTIR spectrometer (Bruker, Billerica, MA) in the attenuated total reflectance (ATR) mode with a diamond crystal using 100 scans per spectrum and a resolution of 4 cm^{-1} and a spectral range of 4000–400 cm^{-1}.

Both ^{29}Si high-power decoupled (HPDEC) and ^{13}C cross-polarization (CP) solid-state magic angle spinning nuclear magnetic resonance (MAS NMR) spectra were recorded using a Bruker DRX-400 WB NMR spectrometer (Bruker Biospin, Karlsruhe, Germany) equipped with a 4-mm MAS BB X/^{1}H probe operating at a Larmor frequency of 79.49 MHz for ^{29}Si, 100.62 MHz for ^{13}C, and 400.15 MHz for ^{1}H, respectively. The spectra were acquired at a spinning speed of 12 kHz and a temperature of 20 °C using tetramethylsilane (TMS) at 0 ppm as external reference. For the HPDEC measurements, 512 scans were collected with a $\pi/2$ pulse of 6.75 µs on ^{29}Si and a recycle delay of 60 s. A SW_f-TPPM heteronuclear decoupling was used during the acquisition. For the CP measurements, 1024 scans were accumulated. During the contact time of 2 ms, a linearly ramped pulse was applied to fulfill the Hartmann-Hahn condition for polarization transfer from protons to carbons. The $\pi/2$ pulse was 2.5 µs on ^{1}H and the recycle delay was set to 5 s. A SW_f-TPPM heteronuclear decoupling was used during the acquisition.

The thermal stability of the hybrid materials with respect to the as-synthesized and silane-functionalized silica was analyzed via thermogravimetric analysis (TGA) using a STA 409 thermobalance (Netzsch, Selb, Germany). The thermal weight losses of samples were measured from room temperature to 800 °C at a heating rate of 10 °C min^{-1} in a stream of atmospheric air. The grafting yield of the polymer fragment in the range of 200–800 °C was calculated by excluding the wt.% loss of the silane linkers according to the following equation [19]:

$$\text{Grafting yield} = \frac{\text{awt\%} - \text{bwt\%}}{\text{rwt\%}} * 100 \quad (1)$$

where $a_{wt\%}$, $b_{wt\%}$, and $r_{wt\%}$ are the weight loss of the hybrid particles, silane-functionalized particles, and residue weight of particles, respectively. The chemical compositions of the synthesized materials (wt.% of carbon, nitrogen, and hydrogen) were examined from CHN elemental analysis (Vario EL III, Elementar Analysensysteme, Langenselbold, Germany). The grafted amount of polymer (wt.%) was also estimated based on elemental analysis data using the following equation [20]:

$$\text{PNIPAM wt.\%} = \left(\frac{\text{N}}{\text{N}^{\circ}}\right) \times 100 \quad (2)$$

where N and N^{o} are the wt.% of nitrogen content in the grafted and as-synthesized copolymer (dried gel) determined by elemental analysis, respectively.

Nitrogen (N_2) physisorption measurements were performed using a Quantachrome Autosorb iQ (Quantachrome, Boynton Beach, USA). Prior to the sorption measurements, all samples were treated under vacuum at 50 °C for 20 h. The specific surface areas (S_{BET}) were calculated using the Brunauer-Emmett-Teller (BET) method in the range of p/p_0 = 0.05–0.35 and the total pore volume was obtained at the maximum relative pressure p/p_0 = 0.98. The nonlocal density functional theory (NLDFT) method was applied to estimate the pore diameters using the adsorption branch model considering N_2 sorption at −196 °C in silica with cylindrical pore geometry.

For comparison to the nitrogen physisorption technique, positron annihilation lifetime spectroscopy (PALS) analysis was done. Before conducting PALS measurements, the samples were annealed in the PALS measurement chamber at 80 °C for 12 h at ~ 3×10^{-5} mbar to remove adsorbed moisture from the surface. About 0.4 ml of as-synthesized, silane-modified, and polymer-grafted silica was placed in the space around a ^{22}Na positron source (activity of ~ 5 µ Ci) in a suitable sample holder. A 4-tube digital (10-bit DC252 digitizer) positron lifetime spectrometer containing four identical conical EJ232 plastic scintillation detectors of Ø1 = 19 mm, Ø2 = 40 mm, and h = 28 mm and custom-made dual high-voltage and coincidence units have been used for PALS measurements around the sample-source arrangement. The maximum time interval between signals from the detectors was set to 1.1 µs (1 µs as coincidence value and 0.1 µs as delay due to cables and data transfer) with a channel width of 50 ps. The obtained count rate was ~ 220 cps (because of the low-activity source) and the time resolution was ~ 175 ps full

width at half maximum (FWHM). The measurement was carried out at 25°C with 3×10^7 counts. The evaluation of the results was carried out using the program MELT (Maximum Entropy for Lifetime Analysis) [21]. It considers the lifetime spectrum as a pseudo-continuous lifetime distribution (it uses a dense lifetime grid) and calculates the intensity for each lifetime depending on the entropy weight. The resulting lifetime distribution is comparable to a pore width distribution without the need to carry out a previous nitrogen physisorption measurement. The pore width was calculated based on the extended Tao-Eldrup (ETE) model to describe the pick-off decay [22]. The pore size determination was carried out by using the Excited Energy Levels and Various Shapes (EELViS) code [23] and cylindrical pore shape with $\Delta = 0.18$ nm.

Small-angle powder x-ray diffraction (XRD) patterns were recorded using a D8 Advance diffractometer (Bruker AXS, Karlsruhe, Germany) (Cu-K_α radiation $\lambda = 1.54$ Å, LynxEye one-dimensional silicon strip detector) in the range $2\theta = 0.4$–$10.0°$ with a step size of 0.01° and a counting time of 1 s/step. The effect of the polymer grafting process on the ordered mesopore structure of the synthesized hybrid materials was studied in comparison to the as-synthesized and silane-functionalized silica. The morphology of the particles was examined using a Leo Gemini 1530 scanning electron microscope (SEM) (Zeiss, Oberkochen, Germany) and JEM2100Plus transmission electron microscope (TEM) (JEOL, Tokyo, Japan). The particle size distribution from the TEM measurement was calculated by using ImageJ software. Energy-dispersive X-ray spectroscopy (EDS) (Bruker NanoLab200, USA) was performed to demonstrate the elemental distributions in the hybrid material.

Results and discussion

Structural characterization of the hybrid materials

FTIR spectroscopy was performed to study the surface chemistry of the synthesized composite particles in contrast to the as-synthesized and silane-functionalized samples (Fig. 2). The surface chemistry of MSNs and MPS-functionalized MSNs was investigated in detail in our previous work [16]. Likewise, the functionalization of the outer surface of MSNs with VTMS was performed following the postsynthetic modification route implemented in our previous work. The FTIR spectra of MV1T showed a signal at 1410 cm^{-1} for the vinyl ($CH{=}CH_2$) in-plane deformation vibrations (Fig. 2b). The broad bands at around 3440 cm^{-1} can be assigned to the stretching vibration of surface silanol groups or surface bound moisture ($SiO–H\ldots H_2O$). Moreover, the stretching of the vinyl groups at 1638 cm^{-1} is overlapping with the O–H assymetric stretching bands of hydrogen-bonded water molecules indicating the successful chemical binding of VTMS on the surface of silica. In addition, the bands at around 3440 cm^{-1} decreased following VTMS functionalization [24].

Therefore, the MPS-modified samples (MM1E/MM1T) are becoming more hydrophilic due to oxygen rich and polar nature of the acrylate functional groups compared to the VTMS-modified sample (MV1T) containing non-polar vinyl groups.

Upon polymerization on the surface of MPS- or VTMS-functionalized MSNs, the silica framework of the hybrid particles remained unchanged. In turn, the characteristic bands of the silica network at 1100 cm^{-1} and 840 cm^{-1} (Si–O–Si asymmetric and symmetric stretching vibrations of the dense silica network, respectively), and 970 cm^{-1} (Si–OH bending vibrations) [24, 25] are preserved after polymer coating (Fig. 2). Furthermore, as shown in Fig. 2a, the hybrid particles synthesized using only NIPAM homo-monomer ($MM1E\text{-}PNM_{0\%}$) displayed a high intense peak at 1638 cm^{-1} (amide carbonyl (C=O) stretching) which is evolved over the C=C stretching peak of silane-functionalized MSNs. The bands at 1539 cm^{-1} (secondary amide (–N–H) bending) and 1462 cm^{-1} (bending of C–H for the methyl ($–CH_3$) groups) vibrations belong to the characteristic peaks of the PNIPAM polymer. The twin bands at 1390 and 1370 cm^{-1} are attributed to the C–H bending vibration of the isopropyl groups ($–CH(CH_3)_2$). The secondary amide (–N–H) and hydroxyl groups (–O–H) stretching bands are observed in the range of 3700 to 3200 cm^{-1} [24, 26]. A broad peak from 2826 to 3000 cm^{-1} is generated by the aliphatic C– H stretching vibration of the grafted polymer in addition to the propyl acrylate molecules of the organosilane-treated samples. The appearance of these intense characteristic absorbance bands of PNIPAM for all samples (Fig. 2) is indication for the chemical grafting of the

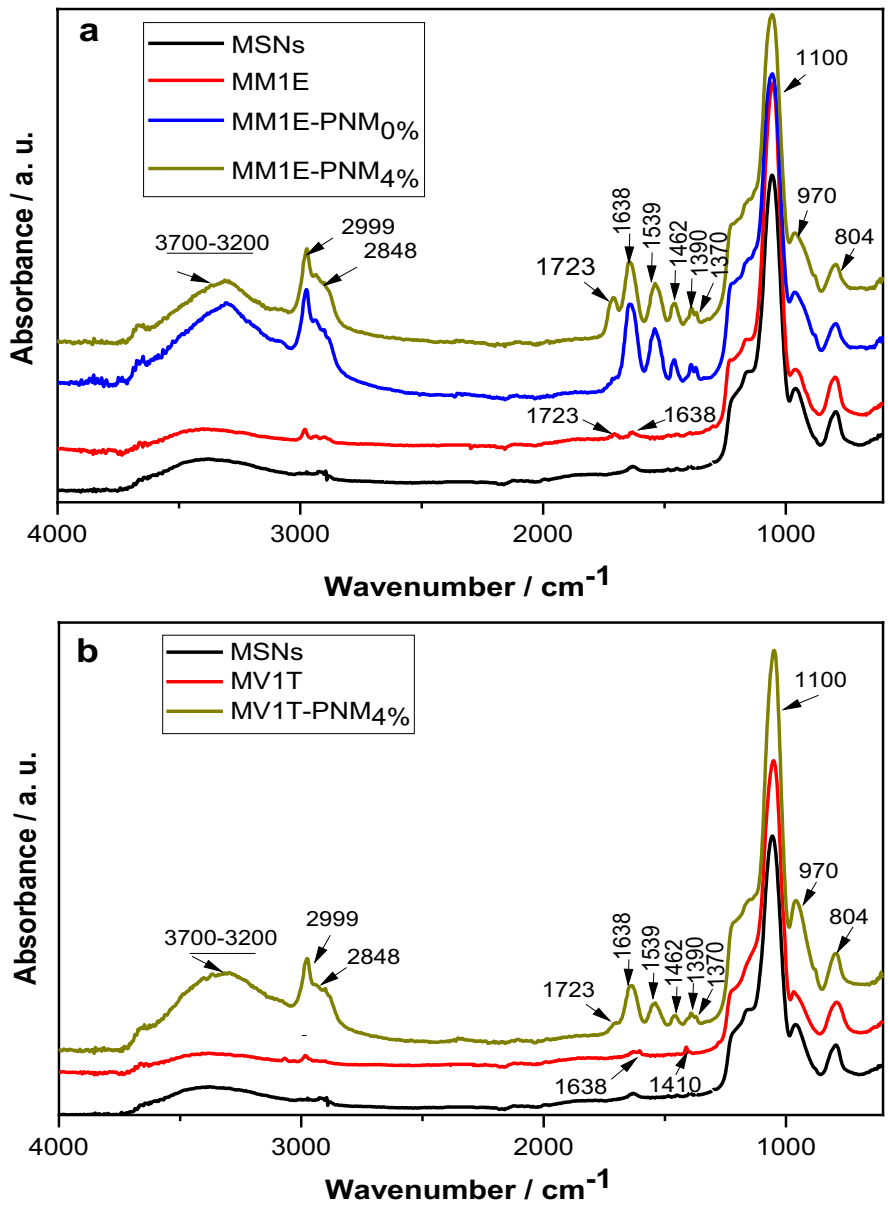

Fig. 2 ATR-FTIR spectra of hybrid materials of PNIPAM homopolymer (MM1E-PNM$_{0\%}$), and PNIPAM-co-MAA copolymer (MM1E-PNM$_{4\%}$ and MV1T-PNM$_{4\%}$) grafted on silane (MPS (**a**) or VTMS (**b**)) functionalized MCM-48-type silica

polymer on the surface of silica. Thus, FTIR spectroscopy provided clear evidences for the step-by-step surface modification and the successful preparation of the hybrid nanoparticles.

Moreover, a sample prepared via adding MAA as a co-monomer (MM1E-PNM$_{4\%}$) showed an apparent increase of the absorption band at around 1723 cm^{-1}. The band corresponds to the carbonyl stretching of the carboxylic acid groups (–COOH) from the co-monomer chains that merely overlapped with the carbonyl stretching vibration of the acryloxy groups (CH_2=CH–COO–) of MPS [27]. The increase of this characteristic band in contrast to MM1E-PNM$_{0\%}$ and its appearance in MV1T-PNM$_{4\%}$ (Fig. 2b) confirmed the successful copolymerization of NIPAM and MAA, and grafting on the surface of silica. Besides, the surface characteristics of the hybrid materials synthesized via polymerization on the surface of silica functionalized with VTMS and MPS are merely identical, regardless of the content of reactive vinyl groups (Fig. 2). Therefore, the chain length of the linker molecule has no pronounced influence on the

characteristic peak intensities that can be correlated to the content of polymer grafted on the silica surface.

A study by Yismaw et al. [16] concerning the silane functionalization of samples prepared under diverse conditions showed clear differences in the concentration of silanes grafted on the surface of silica. As it was calculated based on the external surface area of the as-synthesized MSNs, MM-Co_{35} sample partakes higher silane content (40 molecules nm^{-2}) in contrast to MM1T (29 molecules nm^{-2}) and MM1E (16 molecules nm^{-2}). To investigate the effect of silane content on the final amount of grafted polymer, polymerization was performed on all samples, keeping other conditions identical. For example, the characteristic FTIR peak intensities for MM1E-$PNM_{0\%}$/MM1E-$PNM_{4\%}$ in Fig. 2a and MM1T-$PNM_{0\%}$/MM1T-$PNM_{4\%}$ (Figure S1) samples are inversely correlated with the silane content. When the concentration of silane species was higher (MM1T), the amount of polymer grafted on the silica surface was low as verified in this work. This negative influence can be attributable to the steric hindrance of the nearly bound silane molecules that limit the polymer grafting content. Additionally, in the case of high silane concentrations, the complete outer surface is coated with a thick layer of precondensed silane species. This can prevent the formation of the second layer of polymer species. The results obtained from FTIR spectra are supported by TG and CHN elemental analysis.

^{29}Si and ^{13}C solid-state NMR measurements were performed for a selected hybrid sample (MM1T-$PNM_{4\%}$) to further confirm the chemical grafting of the copolymer on the surface of silica as well as to assess the structure of MSNs after the polymerization process. As shown in Fig. 3a, the ^{13}C CP-MAS NMR spectrum of MM1T-$PNM_{4\%}$ contained characteristic signals for all carbon atoms present in the copolymer structure corresponding to the non-grafted cross-linked copolymer ($PNM_{4\%}$). The typical peaks appeared at 23.4 ppm (–CH_3, c), 36.0 ppm (–CH_2–, d), 44.2 ppm and 48.1 ppm (–CH–, e and e′, respectively), 61.1 ppm (–O–CH_3, f), 68.9 ppm (–CH_2–O–, g), 177.9 ppm (–C=O, h), and 183.3 ppm (–COOH, i) further confirm the successful grafting of the copolymer on the surface of silica [28]. Moreover, the characteristic peaks of the reactive vinyl functional groups of MM1T at 128.1 ppm (CH_2=C–) and 138.7 ppm (–C=CH_2) [16] nearly disappear as a result of its reaction with the NIPAM and MAA monomers. In addition, the decrease of these characteristic peaks further confirms the absence of residual monomers and cross-linkers in the synthesized hybrid materials, hence its complete conversion into a polymer network. The carbonyl peak at 177.9 ppm for MM1T-$PNM_{4\%}$ appears broadened due to the carboxylic groups (–COOH) peak at 183.3 ppm, further suggesting the copolymerization of MAA units into the PNIPAM polymer chain during the polymerization process. Furthermore, the ^{13}C NMR spectra signals assigned to the carboxylic acid units of the comonomer/MAA derivatives are nearly overlapped with the NIPAM segments. The as-synthesized PNIPAM homopolymer ($PNM_{0\%}$) and PNIPAM-co-MAA copolymer ($PNM_{4\%}$) were used as references (Fig. 3a).

The ^{29}Si HPDEC-MAS NMR spectra of MM1T-$PNM_{4\%}$ (Fig. 3b) exhibit two well-resolved peaks at −101.8 ppm and −110.5 ppm usually assigned to Q^n signals of free silanols ($SiOH(SiO)_3$; Q^3) and siloxane ($Si(SiO)_4$; Q^4) structures of silicon, respectively, alike to the as-synthesized (MSNs) and silane-functionalized (MM1T) silica [29, 30]. Additionally, the downfield signals for the organosiloxane species assigned to T^2 ($SiR(OR')(OSi)_2$; −55 to −60 ppm) and T^3 ($SiR(OSi)_3$; −60 to −70 ppm) are observed after the polymer grafting process. The relative concentrations of Q^n and T^n silicon sites in all samples are quantified by deconvoluting the ^{29}Si HPDEC-MAS NMR spectra into individual Lorentzian/Gaussian peaks assuming the peak area is proportional to the concentration of the corresponding silicon sites [31]. The spectra signals and the corresponding relative peak areas for MSNs, MM1T, and MM1T-$PNM_{4\%}$ samples are listed in Table 2.

Moreover, the quantification of the peaks reveals different values with the domination of Q^3 and Q^4 sites for all samples (Table 2). It was noticed that a slight decrease in the percent peak area of Q^3 or Q^2 which was accompanied by merely identical Q^4 percent peak area values after sequential silica surface modification process. This indicates a decrease in the amount of surface free silanol groups (Si–OH) as a result of its condensation and incorporation of the organic moieties. However, excess amount of Q^3 structure is still acquired even after the polymerization process, because the corresponding species are mainly located in the inner pore channels of silica.

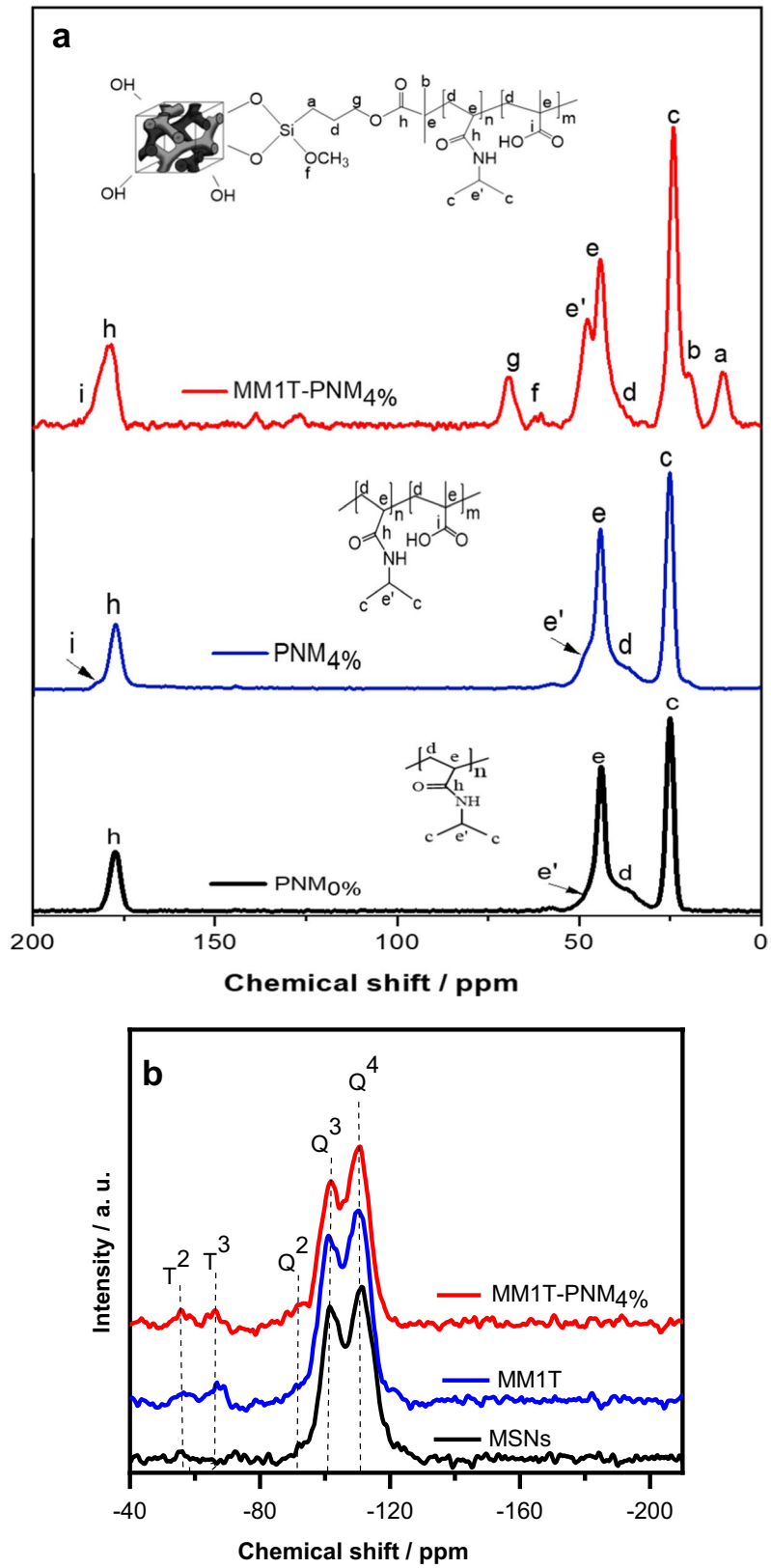

Fig. 3 (**a**) ^{13}C solid-state NMR spectra of as-synthesized polymer ($PNM_{0\%}$/$PNM_{4\%}$) and silica-copolymer hybrid material (MM1E-$PNM_{4\%}$). (**b**) ^{29}Si solid-state NMR spectra of as-synthesized (MSNs), silane-modified (MM1T), and polymer-grafted (MM1T-$PNM_{4\%}$) silica samples

Table 2 Quantification of T^n and Q^n silicon sites based on the peak area analysis of ^{29}Si HPDEC-MAS NMR spectra

Sample	T^2 (%)	T^3 (%)	Q^2 (%)	Q^3 (%)	Q^4 (%)
MSNs	-----	-----	1.8	43.2	55.0
MM1T	4.6	4.9	1.6	35.7	53.2
MM1T-$PNM_{4\%}$	5.4	6.3	1.1	32.3	53.9

The investigated structural observations are consistent with previous reports of MAS NMR spectra for poly(p-phenylenevinylene) polymer-grafted MSNs [30]. A consistent appearance of Q^4 signal is an indication of a stable connectivity within the silica framework which is in agreement with the results of XRD discussed below (Fig. 6). Also, the concentration of T^2 and T^3 structural signals of silicon sites (approximately 10%) of silane-functionalized particles remained unaltered by the polymerization process. This result provides further evidence that the polymer grafting reaction indeed took place during the hybrid material synthesis. The correlation of the ^{29}Si and ^{13}C NMR spectroscopy results reveals the coexistence of silica framework and a polymer network within the hybrid materials.

Effect of reaction parameters on the final polymer content

The dependence of the net polymer content on the surface of silica with respect to various reaction parameters (monomer/co-monomer amount, silane linker content and its type, and reaction time) was studied by TG and CHN elemental analyses. Fig. 4a shows the percent weight loss (wt.%) from bare MSNs and MSNs with different silane contents (MM1E, MM1T, and MM-Co_{35}) as well as its subsequent copolymer-grafted (MM1E-$PNM_{\mathbf{4\%}}$, MM1T-$PNM_{\mathbf{4\%}}$, and MM-Co_{35}-$PNM_{\mathbf{4\%}}$) hybrid materials. The content of MPS coupling agents on the outer surfaces of silica was modulated by varying the solvent type and surface modification routes [16]. Furthermore, in this work, the degree of polymerization from low to high silane linker contents on the surface of silica was investigated. For all samples, the percent weight loss below 200 °C is associated with the evaporation of physically adsorbed components including the mass of trace organic matter and moisture.

A higher weight loss was recorded for polymer-grafted samples (MM1E-$PNM_{4\%}$: 41%, MM1T-$PM_{4\%}$: 36%, and MM-Co_{35}-$PNM_{4\%}$: 42%) in comparison to silane-modified (MM1E: 11%, MM1T: 17%, and MM-Co_{35}: 20%) and bare MSNs (3%) in the temperature range from 200 to 800 °C as expected (Fig. 4a). This is attributed to the decomposition of the grafted copolymer into ammonia and CO_2 besides the silane linker organic fractions and dehydration of the surface silanol groups from the silica surface [32]. The grafting yield of the polymer organic fragment in the range of 200–800 °C was calculated according to Eq. 1 by excluding the wt.% loss of silane linker as summarized in Table 3. This is because each sample contains a different amount of silanes, which can affect the accurate quantification of the grafted polymer. Hence, the grafting yields of the polymer from low (MM1E-$PNM_{4\%}$), moderate (MM1T-$PNM_{4\%}$), and high (MM-Co_{35}-$PNM_{4\%}$) concentrations of silane linker groups were calculated to be 36.6, 25.0, and 30.1 wt.%, respectively. Comparably, the composite nanoparticles prepared using VTMS as a silane linker (MV1T-$PNM_{4\%}$) showed a grafting yield of 33.3% as depicted in Fig. 4b, c. These results suggest that a higher amount of polymer was grafted relatively on silica containing low content of linker molecules, besides the shortest chain length of the linker.

As summarized in Table 3, the polymer grafting yield calculated based on the content of nitrogen from elemental analysis according to Eq. 2 was consistent with the TGA results. The grafted amount of polymer was not directly proportional to the linker concentration on the silica surface. For example, for MM-Co_{35}-$PNM_{4\%}$ sample characterized by relatively high silane content, a low polymer grafting yield (30.1%) was observed in comparison to the polymer grafted from MM1E-$PNM_{4\%}$ sample with low silane linker content. Similarly, Nagase et al. reported that the variable content of surface-grafted initiator has no significant influence on the amount of polymer grafted on the surface [33]. In addition, as shown in Table 3, the chain length of surface-grafted linkers (acryloxy groups of MPS or vinyl groups of VTMS) showed nearly a similar effect on the final polymer content. The values determined from EA are in agreement with TGA results.

Based on the above results, MM1E sample with optimal silane concentration was used to further optimize the other variables influencing the final polymer

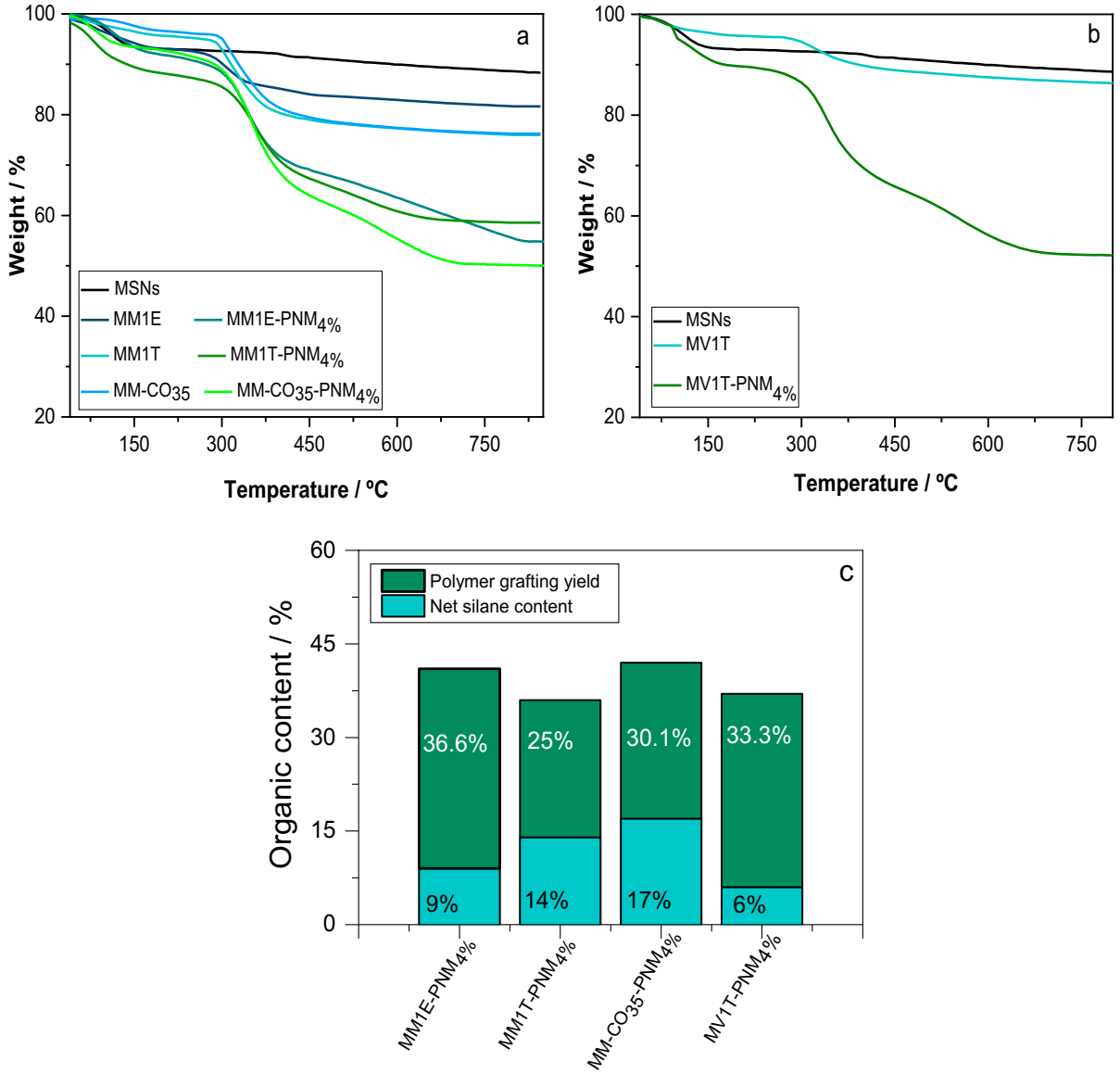

Fig. 4 TGA curves for (**a**) MSNs with different MPS contents (MM1E, MM1T, and MM-Co_{35}) and its subsequent polymer-grafted hybrid particles (MM1E-$PNM_{4\%}$, MM1T-$PNM_{4\%}$, and MM-Co_{35}-$PNM_{4\%}$), (**b**) VTMS-functionalized (MV1T) MSNs and its hybrid particles (MV1T-$PNM_{4\%}$), (**c**) polymer grafting yield (%) with respect to the net silane content (wt.%) and type

content. The variations in the initial feed ratio of NIPAM and MAA and reaction time and the corresponding polymer content determined from elemental analysis are presented in Table S1. The content of carbon and nitrogen in the hybrid particles raises with an increase in the initial feed ratio of NIPAM under the same reaction conditions (Table S1). This is because the high monomer concentration increases its availability for the polymerization process. As a result, larger growing polymer chains are formed and the PNIPAM content on the silica surface increased. Generally, a high content of the grafted copolymer led to good outer surface coverage and helps to control the pore opening and closing mechanism for the desired application. Therefore, precise control of the location of the polymer aids to overcome partial or complete blockage of the pores. Thus, 7.95 mmol of NIPAM was considered as an optimal amount for

Table 3 Content of copolymer grafted onto the MCM-48 silica surface containing different amounts/types of organosilanes

Sample	Δm [*Wt.%*][a]	X_P [%][a]	X_{EC} [%][b]			X_P [wt.%][b]
			C	H	N	
MM1E-PNM$_{4\%}$	41	36.6	25.0	4.2	4.0	36
MM1T-PNM$_{4\%}$	36	25.0	20.3	4.0	2.5	23
MM-Co$_{35}$-PNM$_{4\%}$	42	30.1	28.0	5.0	3.4	30
MV1T-PNM$_{4\%}$	37	33.3	24.2	4.6	4.0	36
PNM$_{4\%}$	--------	--------	58.6	9.8	11.0	--------

[a]Weight loss from 200 to 800 °C (Δm) and polymer grafting yield (X_P) estimated from TGA. [b]Elemental composition (X_{EC}) of dry pristine polymer (PNM) and composite materials, and grafted amount of polymer (X_P) estimated from elemental analysis

the synthesis of the hybrid materials. However, varying the concentration of the co-monomer (MAA) resulted in nearly the same elemental compositions (Table S1). Thus, it has no pronounced effect on the final polymer content since the concentration considered is very low. In order to control the degree of polymerization on the surface of silica, the polymerization was conducted for different time periods (3 h, 6 h, 12 h, and 24 h), keeping all other variables constant. As shown in Table S1, elemental analysis revealed nearly the same amount of grafted polymer when the polymerization time is elongated from 3 to 24 h. Thus, in this work, a reaction period of 6 h was applied as an optimum time for complete monomer conversion during polymerization process since further extending of reaction time had no effect.

A selected hybrid material sample (MM1E-PNM$_{4\%}$) with an optimum polymer amount was considered for further SEM/TEM, XRD, N_2 sorption, and PALS analysis studies.

Morphology, particle size, and core-shell structure

SEM and TEM micrographs (Fig. 5) showed the morphology of MM1E-PNM$_{4\%}$ in comparison to MSNs. After polymer grafting, the spherical particle morphology was basically preserved. The surface appeared homogenous despite slight interparticle aggregation that limited its dispersion in a dry state. The average particle size measured from the SEM image using *ImageJ* software for MM1E-PNM$_{4\%}$ is 349 nm ± 26 (Fig. 5b). As expected, this is slightly larger than the as-synthesized MSNs (~ 295 nm) (Fig. 5a). Well-defined uniform core-shell structured nanospheres with an average particle size of 367 nm ± 25 and shell thickness around 29 nm ± 8 are also clearly visible in the TEM image (Fig. 5d) for MM1E-PNM$_{4\%}$. Hence, the average particle size measured from TEM micrograph for MSNs ~ 306 nm was increased to ~ 367 nm after polymer grafting. The spheres show a noticeable contrast between the darker core silica and bright/gray uniform edges of a thin polymer shell [34]. The analysis of particle size distribution by TEM clearly revealed spheres with relatively narrow distribution (Fig. 5e).

The final well-dried hybrid particles were aggregated unlike the finely dispersed powders of the as-synthesized and silane surface-modified silica. In this work, the aggregation of the material was found to be dependent on the amount of cross-linker (MBA) used during the synthesis. Taking this into consideration, different amounts of cross-linker (0.1 mmol, 0.2 mmol, 0.3 mmol, and 0.4 mmol) were used for the above reaction mixture. For lower cross-linker concentration (0.1 mmol), loosely aggregated particles formed. Increasing the cross-linker concentration from 0.1 to 0.4 mmol produced strongly physically aggregated final products. Hence, low amount of cross-linker (0.1 mmol) was used throughout this work. Furthermore, both the SEM and TEM images (Fig. 5b, d) clearly showed that the composite particles prepared using low cross-linker amount were loosely aggregated possibly by (1) chemically cross-linked network of the polymer chains produced by the bi-functional cross-linkers or (2) physically cross-linked network due to entanglements of the polymer chains on the adjacent silica surface [34]. In addition, the physical networks can be formed by molecule-molecule interactions like hydrogen bonds and van der Waals interactions. Overall, the SEM/TEM images (Fig. 5a–d) confirmed that the nanoparticles maintained their

original morphology upon polymer grafting and the long treatment procedure.

EDS elemental analysis was performed for a selected core-shell structure material sample (MM1E-$PNM_{4\%}$) and demonstrates the elemental distribution in the hybrid structure. EDS results (Fig. 5f) revealed the presence of carbon and nitrogen in the silica-polymer hybrid material with silicon and oxygen as the major elements. The high content of carbon and presence of nitrogen in the hybrid material are indications of the presence of the polymer coating. Overall, this result further confirmed the grafting of the polymer on the silica surface. EDS elemental mapping of carbon and silicon (Fig. 5g) of a single sphere shows the enrichment of the carbon signal at the outer shell of the particle. Thus, the existing core-shell structure can be shown in addition to the TEM imaging.

Impact of polymer grafting on the ordered pore structure and textural properties of MCM-48-type silica

Small-angle XRD patterns of MM1E-$PNM_{4\%}$ showed narrow sharp peaks at 2θ values of roughly 2.7° and 3.1° and two small diffraction peaks at around 4.8° and 5.1° (Fig. 6). These peaks correspond to (211), (220), (420), and (332) lattice planes, respectively. The characteristic patterns are consistent with the one of the typical highly ordered 3D cubic MCM-48 silica structures reported in literature [12, 14] and result from the periodicity of the pore structure, which possesses a cubic symmetry (space group Ia-3d). This proves that the long-range ordered mesoporous structure is well preserved after polymer grafting despite the lower intensity and slight peak shift to higher 2θ value in contrast to MSNs and MM1E samples (Fig. 6). The decrease in peak intensities can be due to the limited long-range order of mesopores of silica following polymer grafting [14]. The peak shift to higher angles results from the pore covering/filling effect by the polymer units, which causes a decrease in pore size. This further leads to a decrease in the long-range ordered arrangement of the smaller mesopores. Nevertheless, as shown in Fig. 6, the diffraction peaks of MCM-48 silica are well preserved even after the long polymer grafting process, which indicates the ordered mesopore structure of silica core was maintained after covering of the outer surface with copolymer. From the well-resolved (211) and (220) peaks, the following unit cell parameters were calculated for the three samples shown in Fig. 6: MSNs a = 83 Å, MM1E a = 85 Å, and MM1E-$PNM_{4\%}$ a = 81 Å.

The nitrogen physisorption isotherms of the hybrid materials (MM1E-$PNM_{4\%}$ and MV1T-$PNM_{4\%}$) displayed a typical type IV isotherm (Fig. 7a, c), comparable to MSNs and silane-functionalized (MM1E and MV1T) samples [35]. Well-preserved isotherms further confirm that the structure of ordered mesoporous silica particles stays intact after a long polymer grafting process. The corresponding textural properties of all samples are summarized in Table 4. The average pore width (NLDFT method, adsorption branch) of MSNs sample was reduced from 3.4 to 3.1 nm succeeding polymer grafting (MM1E-$PNM_{4\%}$). The BET specific surface area (p/p_0 = 0.05–0.3) and the total pore volume at maximum relative pressure (p/p_0 = 0.9) decreased from 1093 to 835 $m^2\ g^{-1}$ and from 0.74 to 0.5 $cm^3\ g^{-1}$, respectively, in comparison to MM1E. No significant pore blockage was observed from porosimetry analysis, i.e., more than 75 % of specific surface area, 68 % total pore volume, and the mean pore diameter were retained after successful grafting of the polymer. The slight reduction of specific surface area, pore volume, and mesopore diameter could be associated with the grafting of polymer chains into the pore entrance which leads to a slight pore blockage. This minor decrease in porosity values confirmed the successful grafting of the polymer mainly on the outer surface of silica particles previously functionalized by silanes. A similar trend was also observed for MV1T-$PNM_{4\%}$ sample (Table 4 and Fig. 7c, d). In this work, the porosity values determined for MCM-48 structure silica-polymer hybrid materials, where the polymerization processes took place preferentially on the outer surface of silica, are higher compared to previous reports for different types of MSNs [14]. To verify the contribution of the grafted polymer on the textural properties, a pristine copolymer of PNIPAM-co-MAA ($PNM_{4\%}$) was measured and did not show any adsorption properties (Fig. 7a, b). The pristine polymer revealed an isotherm where the adsorbed volume of nitrogen is found to be perfectly linear over the whole p/p_0 range. Thus, the observed specific BET surface area (4 m^2/g), total pore volume (0.001 cm^3/g), and average pore width (0.7 nm) of the polymer are negligible in the composite material. Overall, the porosity

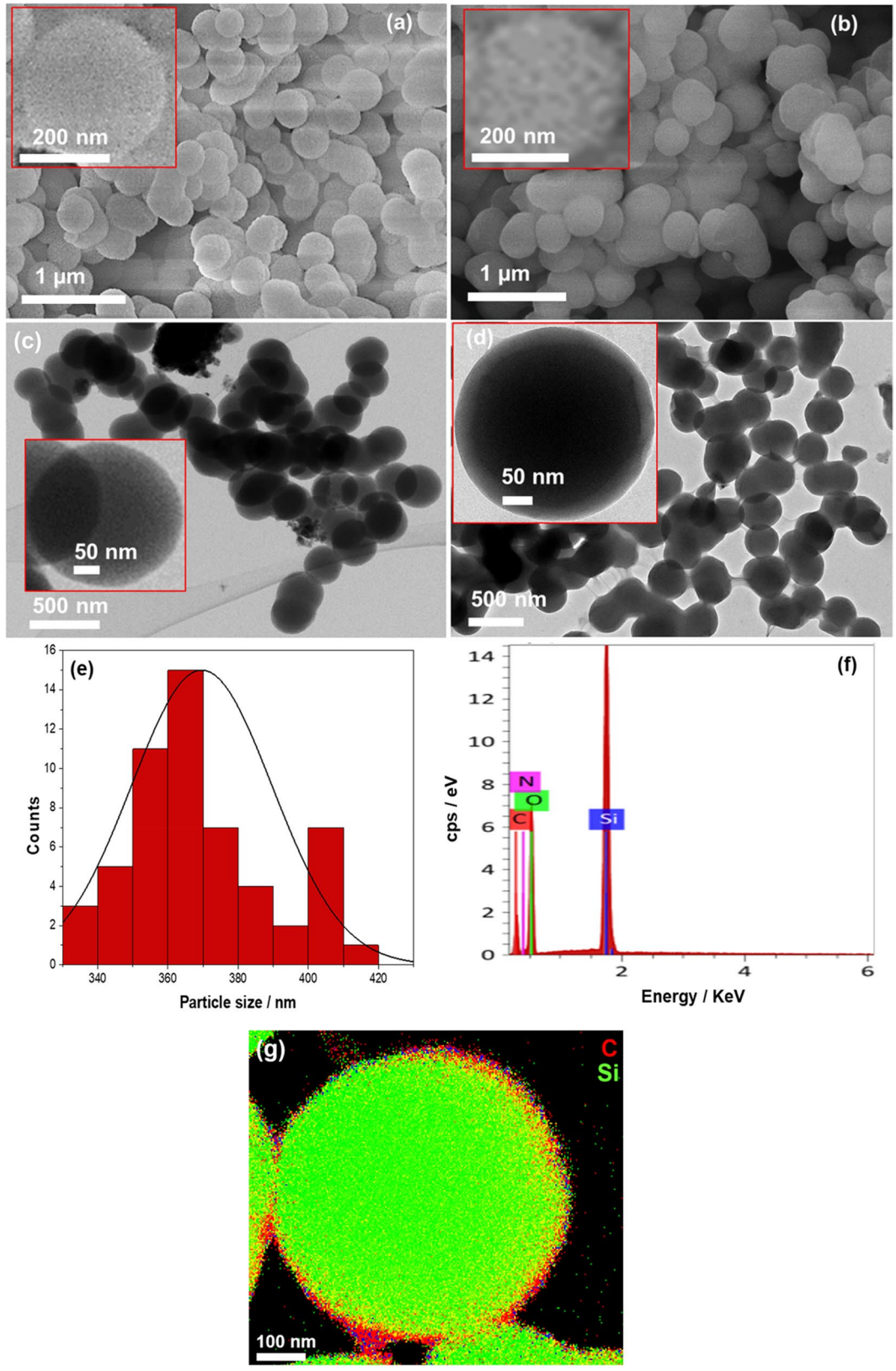
(a)
200 nm
1 µm
(b)
200 nm
1 µm
(c)
50 nm
500 nm
(d)
50 nm
500 nm
(e)
Counts
Particle size / nm
(f)
cps / eV
Energy / KeV
N
O
C
Si
(g)
C
Si
100 nm

◂**Fig. 5** SEM and TEM images of as-synthesized (**a** and **b**: MSNs) and the corresponding copolymer-grafted nanoparticles (**b** and **d**: MM1E-PNM$_{4\%}$), respectively. (**e**) and (**f**) are the particle size distribution based on the TEM measurement and EDS spectra of the hybrid material, respectively. STEM elemental mapping of carbon and silicon (MM1E-PNM$_{4\%}$) is shown in (**g**)

parameters of the hybrid materials (Table 4) are optimal values for the desired application.

PALS is a widely used and powerful technique of porosimetry [36, 37] and it provides complementary information to standard porosimetric tools [38, 39]. So, in the current study, PALS analysis was done to detect all the pores present for a given sample and to further investigate the effect of a subsequent surface modification on the mesopore properties. The as-synthesized MSNs exhibit a peak centered at around 2.5 nm in the pore width distribution (PWD) that can be attributed to the primary mesopores (Fig. 8). Furthermore, two additional peaks in PWD at around 0.9 nm (narrow) and 7.5 nm (broad) correspond to the o-Ps annihilation in the free volumes of the pore walls (bulk silica or polymer) and the ortho-positronium (o-Ps) escaped into interparticle spaces, respectively, since the produced o-Ps atoms are able to diffuse through the interconnected pores of the material [40]. As expected, the probability of their diffusion through highly interconnected network of MCM-48 pores outside a particle with size of about 300–350 nm (Fig. 5) is greater than the rate of annihilation in the primary mesopores [41]. As a result, the volume of primary pores is underestimated, while the volume of interparticle spaces is overestimated. However, this effect allows to estimate the accessibility of the primary pores from the outside, which is discussed further. The same number of peaks with aforementioned origins was observed for the organosilane-modified sample (MM1E). The peak related to primary mesopores (~ 2.5 nm) has been increased in intensity in contrast to MSNs. This indicates a decreased accessibility of primary pores to outer particles' surface causing less o-Ps leaving primary pores to interparticle spaces. Such a decreased accessibility of primary pores to interparticle spaces is presented in Table 5, which shows the integrated area under the peak or integrated intensity of the primary pore groups (I_a-primary pores) and interparticle spaces (I_a-interparticle spaces). In turn, the silica-polymer hybrid particles (MM1E-PNM$_{4\%}$) revealed an additional peak at ~ 0.7 nm. This is expected to be the free volume in the cross-linked polymer shell as concluded from TEM images in Fig. 5d.

The peak at ~ 1.1 nm, which was previously attributed to the silica pore walls, showed a pronounced increase in volume after polymer grafting (MM1E-PNM$_{4\%}$). It is typical that there are two or even more peaks in the range of small free volume sizes (< 2 nm) in polymers and polymer hybrids [42]. It is also known that the probability of the o-Ps formation is usually greater in polymers than in silica. Thus, this increase in the 1.1-nm peak can be attributed to an additional pore group present in the polymer with a small contribution from the silica pore walls. This can be also correlated with the change in the packing nature of particles (less compact) as a result of interparticle aggregations after polymer grafting

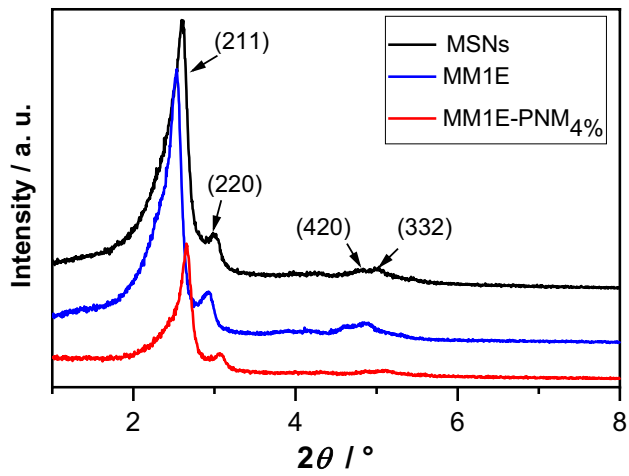

Fig. 6 XRD pattern of MM1E-PNM$_{4\%}$ in comparison to MM1E and MSNs samples

[43], compared to the finely dispersed MSNs and MM1E samples. Alternatively, this peak may be larger due to the coverage of silica by the polymer that prevents o-Ps escape from the pore wall to the pore interior. Worth mentioning, conventional PALS that utilizes energetic ^{22}Na source cannot distinguish between porosity in shell and core. Thus, in addition to the shell polymeric layer, a fraction of polymer may be grafted to the inner channels and this can be examined by inspecting the primary pore signal. The high intense peak that originates from the primary mesopores showed a slight peak shift to smaller pore width (2.5 to 2.2 nm), which demonstrates the occupation of certain part of pore channels of silica by the polymer chains even though it is preferentially grafted on the outer surface of silica. The partial grafting on the inner pore surface is further confirmed by the enhanced intensity of the mesopore signal.

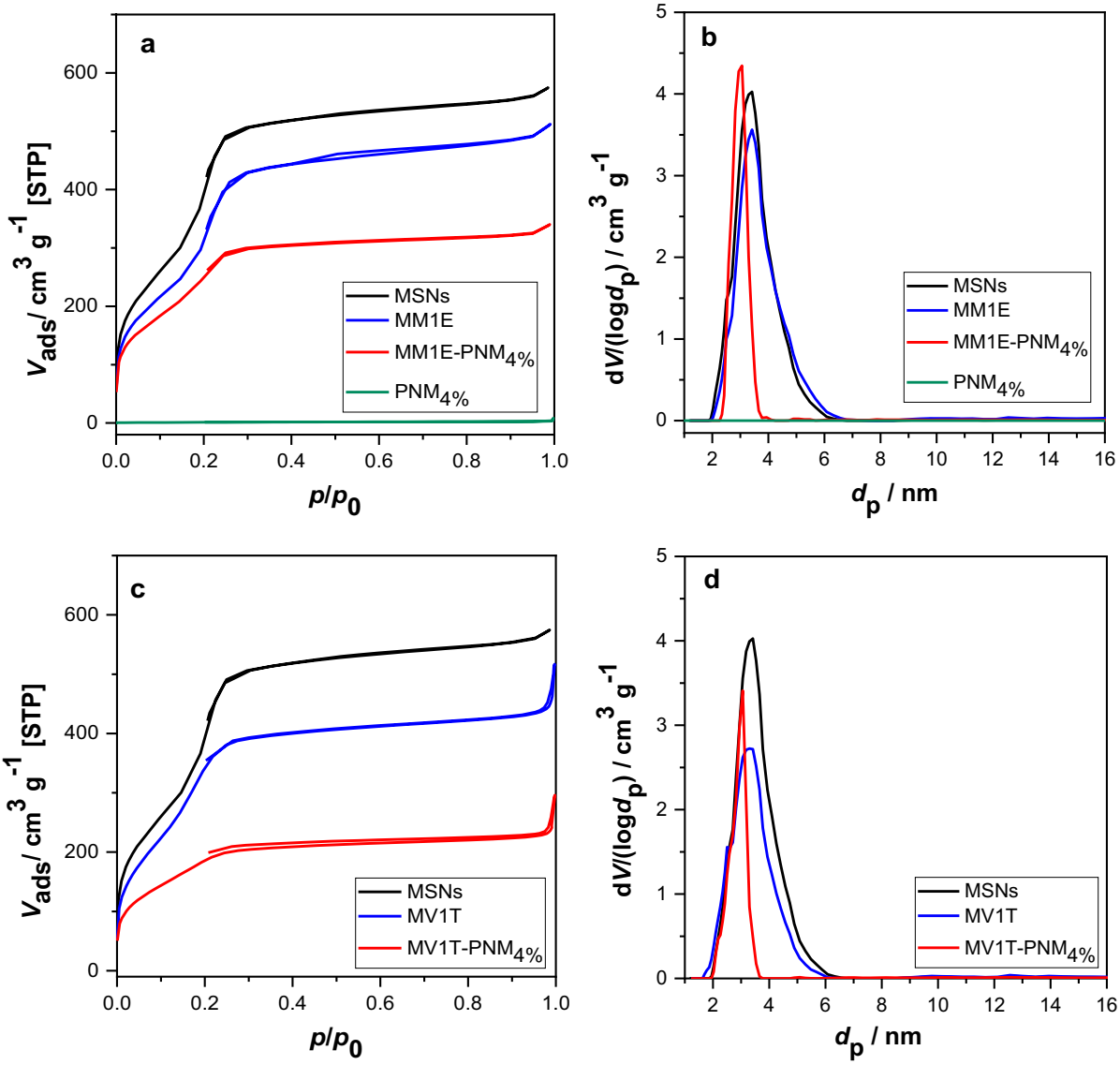

Fig. 7 Nitrogen physisorption isotherms for the as-synthesized silica (MSNs), pristine polymer (PNM$_{4\%}$), MPS (MM1E), and VTMS (MV1T) functionalized and subsequent polymer-grafted (MM1E-PNM$_{4\%}$ and MV1T-PNM$_{4\%}$) silica samples (**a** and **c**). In **b** and **d**, the corresponding pore width distribution curves are shown

Table 4 Textural properties of the as-synthesized (MSNs or polymer), silane-functionalized, and polymer-grafted MSNs

Sample	S_{BET} [$m^2\ g^{-1}$][a]	V_{meso} [$cm^3\ g^{-1}$][a]	d_{meso} [nm][a]
MSNs	1229	0.85	3.4
MM1E	1093	0.74	3.4
MM1E-PNM$_{4\%}$	835	0.50	3.1
MV1T	1147	0.72	3.2
MV1T-PNM$_{4\%}$	722	0.40	3.1
PNM$_{4\%}$	4	0.001	0.7

[a]BET surface area (S_{BET}), mesopore width (d_{meso}), and volume (V_{meso}) based on nitrogen physisorption measurements

Moreover, the increase in the integrated area (which correlated with volume) of this peak (I_a-primary pores in Table 5) can indicate a partial blockage of the pore entrances and a reduction in their availability. This observation is in line with the nitrogen sorption analysis results.

Contrary to primary mesopores, the broad peak related to the interparticle component centered at around 7.5 nm for MSNs is getting sequentially narrower and damped following subsequent modifications (MM1E, ~ 6.7 nm and MM1E-PNM$_{4\%}$, ~ 4.2 nm) (Table S2 and Table 5). This could be caused by the occupation of the interparticle spaces following subsequent surface modification/particle aggregation. Hence, o-Ps measure smaller interparticle spaces because of humps of the organic component (organosilane/polymer) grafted on the outer surface of silica. The damped o-Ps intensity is a result of the occupancy of grafted polymer into the inner channel and their openings (fewer o-Ps atoms can reach the interparticle spaces migrating from the inner porosity).

Overall, based on the results of PALS analysis, it can be concluded that the polymer occupies

Table 5 Integrated peak areas of primary pores (I_a-primary pores) and interparticle spaces (I_a-interparticle spaces) from MELT for MSNs and MM1E and MM1E-PNNM$_{4\%}$

Sample	I_a-primary pore *[a.u.]*	I_a-interparticle space *[a.u.]*
MSNs	0.02	1.02
MM1E	0.06	0.63
MM1E-PNM$_{4\%}$	0.16	0.21

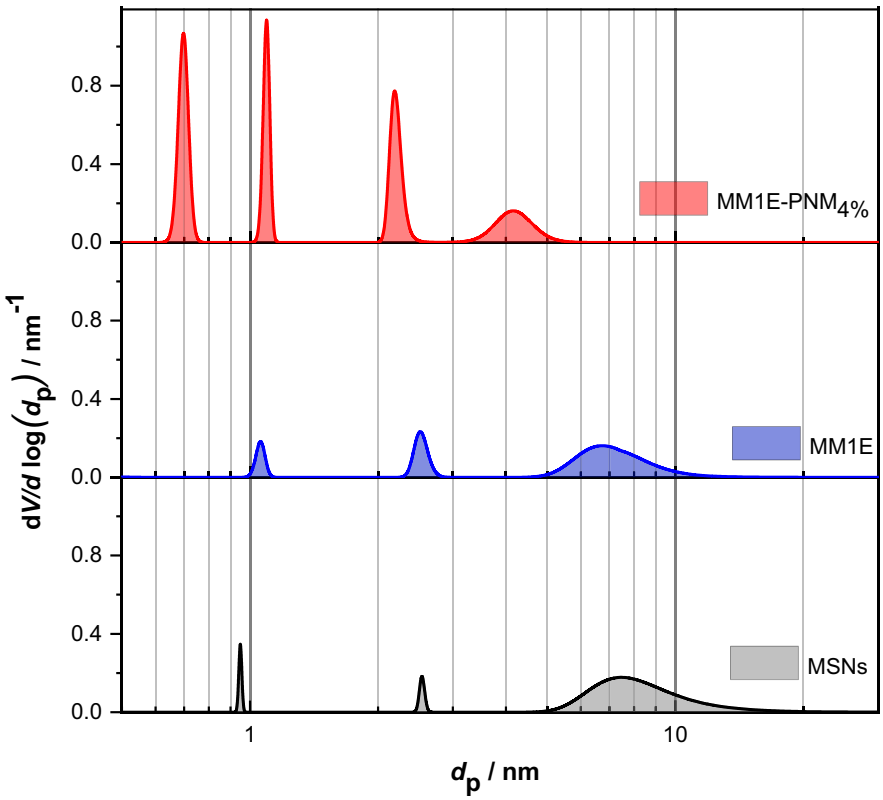

Fig. 8 Pore width distributions of MSNs, MM1E, and MM1E-PNNM$_{4\%}$ samples determined from PALS measurements by MELT

considerable interparticle space. Consequently, the surface area, pore volume, and average pore width were decreased after polymer grafting process as depicted from the nitrogen sorption analysis. The average pore width of the main mesopores, as determined from PALS analysis, is lower (26 %) for all samples in contrast to the nitrogen sorption analysis results calculated based on the NLDFT model (Table 4). This can be attributable to the escape of o-Ps from the main mesopores to the interparticle spaces, which acts as an additional channel of o-Ps decay and causes underestimation of the o-Ps lifetime in the main mesopores. Nevertheless, both analysis techniques showed a trend of slight average pore width reduction of the main mesopores following polymer grafting on the outer surface of silica. The narrow peak of the main mesopores from the PALS analysis corresponds to the N_2 sorption analysis and further confirmed the uniformity of mesopores for all samples. The peak intensity of main mesopores in the PALS measurement is strongly influenced by the o-Ps migration from pore to pore or out of the particles and the connectivity level between primary pores and the particle surface. Hence, deducing the pore volume from PALS results and correlating with the peak intensity is neither absolute nor straightforward [40].

Generally, ordered mesoporous silica-PNIPAM-co-MAA copolymer hybrid materials are successfully designed as a core-shell structure.

Conclusions

MCM-48-type MSNs and PNIPAM-co-MAA copolymer core-shell structured hybrid particles were successfully synthesized by free radical copolymerization. Their physicochemical properties were demonstrated in this study. It was shown that quantitative grafting of the polymer can be tuned in the range 18 to 40 % via adjusting the initial concentration of monomers and other reaction parameters. According to XRD and nitrogen physisorption studies, a high content of polymer was preferentially grafted on the outer surface of silica. Hence, the morphology, ordered mesopore structure, and porosity parameters of core silica were nearly retained after a subsequent surface modification process. The narrow pore width distribution of the main mesopores in silica nanoparticles from the PALS analysis corresponds to the N_2 sorption analysis and further confirmed the uniformity of mesopores. In addition to detecting the grafted polymer, PALS also has shown that the accessibility of inner channels to the outer surfaces is influenced by grafting and inner pore coating and pore blockage is expected. This important finding should be considered during real operation of the core (silica)–shell (polymer) system as it may affect its performance. Moreover, PALS results suggest that the decrease of the size of the interparticle spaces after polymer grafting confirms that the grafting occurs on the outer particle surfaces.

TEM images clearly showed smooth surface core-shell structure hybrid particles with an average particle size of 367 ± 25 nm and the polymer shell thickness of 29 ± 8 nm. The stimuli-responsive phase transition behavior of the composite materials and their potential application for controlled drug delivery will be demonstrated in a subsequent study. Additionally, the high accessibility of the inner pore channels of silica core with high specific surface area and pore volume while the polymer was preferentially grafted on the outer surface can improve the loading capacity of cargo molecules for the planned application study.

Funding This research work was financially supported by the Institute of Chemical Technology, Faculty of Chemistry and Mineralogy, Universität Leipzig, and the German Academic Exchange Service (DAAD).

Compliance with ethical standards

Conflict of interest The authors declare no competing interests.

References

1. Wang Y, Zhao Q, Han N et al (2015) Mesoporous silica nanoparticles in drug delivery and biomedical applications. Nanomedicine Nanotechnology, Biol Med 11:313–327. https://doi.org/10.1016/j.nano.2014.09.014
2. Moraes J, Ohno K, Maschmeyer T, Perrier S (2013) Synthesis of silica–polymer core–shell nanoparticles by reversible addition–fragmentation chain transfer polymerization. Chem Commun 49:9077. https://doi.org/10.1039/c3cc45319g
3. Zhao XJ, Gao ZF, Jiang ZY (2015) A Study of HCl Gas Adsorption/Desorption Properties of PNIPAM Brushes. Macromol Theory Simulations 24:460–467. https://doi.org/10.1002/mats.201500027

4. Cao M, Shen Y, Yan Z et al (2021) Extraction-like removal of organic dyes from polluted water by the graphene oxide/PNIPAM composite system. Chem Eng J 405:126647. https://doi.org/10.1016/j.cej.2020.126647
5. Yadavalli T, Ramasamy S, Chandrasekaran G et al (2015) Dual responsive PNIPAM–chitosan targeted magnetic nanopolymers for targeted drug delivery. J Magn Magn Mater 380:315–320. https://doi.org/10.1016/j.jmmm.2014.09.035
6. Gupta P, Vermani K, Garg S (2002) Hydrogels: from controlled release to pH-responsive drug delivery. Drug Discov Today 7:569–579. https://doi.org/10.1016/S1359-6446(02)02255-9
7. Zheng Y, Wang L, Lu L et al (2017) pH and Thermal Dual-Responsive Nanoparticles for Controlled Drug Delivery with High Loading Content. ACS Omega 2:3399–3405. https://doi.org/10.1021/acsomega.7b00367
8. Li J, Wang L, Benicewicz BC (2013) Synthesis of Janus Nanoparticles via a Combination of the Reversible Click Reaction and "Grafting to" Strategies. Langmuir 29:11547–11553. https://doi.org/10.1021/la401990d
9. Tang F, Li L, Chen D (2012) Mesoporous Silica Nanoparticles: Synthesis, Biocompatibility and Drug Delivery. Adv Mater 24:1504–1534. https://doi.org/10.1002/adma.201104763
10. He Q, Shi J (2011) Mesoporous silica nanoparticle based nano drug delivery systems: synthesis, controlled drug release and delivery, pharmacokinetics and biocompatibility. J Mater Chem 21:5845. https://doi.org/10.1039/c0jm03851b
11. Guillet-Nicolas R, Popat A, Bridot J-L et al (2013) pH-Responsive Nutraceutical-Mesoporous Silica Nanoconjugates with Enhanced Colloidal Stability. Angew Chemie Int Ed 52:2318–2322. https://doi.org/10.1002/anie.201208840
12. He J, Shen Y, Evans DG (2008) A nanocomposite structure based on modified MCM-48 and polystyrene. Microporous Mesoporous Mater 109:73–83. https://doi.org/10.1016/j.micromeso.2007.04.051
13. Kalbasi RJ, Mosaddegh N (2011) Synthesis and characterization of poly(4 vinylpyridine) /MCM-48 catalyst for one-pot synthesis of substituted 4H-chromenes. Catal Commun 12:1231–1237. https://doi.org/10.1016/j.catcom.2011.04.004
14. Meléndez-Ortiz HI, Puente-Urbina B, Ibarra-Vallejo E et al (2018) Polyacrylamide-coated MCM-48 mesoporous silica spheres: synthesis, characterization and drug delivery study. J Porous Mater 25:649–656. https://doi.org/10.1007/s10934-017-0477-z
15. Yismaw S, Kohns R, Schneider D et al (2019) Particle size control of monodispersed spherical nanoparticles with MCM-48-type mesostructure via novel rapid synthesis procedure. J Nanoparticle Res 21:258. https://doi.org/10.1007/s11051-019-4699-7
16. Yismaw S, Ebbinghaus SG, Wenzel M et al (2020) Selective functionalization of the outer surface of MCM-48-type mesoporous silica nanoparticles at room temperature. J Nanoparticle Res 22:279. https://doi.org/10.1007/s11051-020-05006-2
17. Varga I, Gilányi T, Mészáros R et al (2001) Effect of Cross-Link Density on the Internal Structure of Poly(N -isopropylacrylamide) Microgels. J Phys Chem B 105:9071–9076. https://doi.org/10.1021/jp004600w
18. Datta P, Genzer J (2016) "Grafting through" polymerization involving surface-bound monomers. J Polym Sci Part A Polym Chem 54:263–274. https://doi.org/10.1002/pola.27907
19. Peng W, Zhang Z, Rong M, Zhang M (2019) Core-Shell Structure Design of Hollow Mesoporous Silica Nanospheres Based on Thermo-Sensitive PNIPAM and pH-Responsive Catechol-Fe3+ Complex. Polymers (Basel) 11:1832. https://doi.org/10.3390/polym11111832
20. Alli A, Hazer B (2011) Synthesis and Characterization of Poly(N-Isopropyl Acryl Amide)-g-Poly(Linoleic Acid)/Poly(Linolenic Acid) Graft Copolymers. J Am Oil Chem Soc 88:255–263. https://doi.org/10.1007/s11746-010-1663-1
21. Shukla A, Hoffmann L, Manuel AA, Peter M (1997) Melt 4.0 a Program for Positron Lifetime Analysis. Mater Sci Forum 255–257:233–237. https://doi.org/10.4028/www.scientific.net/MSF.255-257.233
22. Ciesielski K, Dawidowicz AL, Goworek T et al (1998) Positronium lifetimes in porous Vycor glass. Chem Phys Lett 289:41–45. https://doi.org/10.1016/S0009-2614(98)00416-3
23. Zaleski R, Wawryszczuk J, Goworek T (2007) Pick-off models in the studies of mesoporous silica MCM-41. Comparison of various methods of the PAL spectra analysis. Radiat Phys Chem 76:243–247. https://doi.org/10.1016/j.radphyschem.2006.03.044
24. Nagappan S, Park SS, Kim BK et al (2018) Synthesis and functionalisation of mesoporous materials for transparent coatings and organic dye adsorption. New J Chem 42:10254–10262. https://doi.org/10.1039/C8NJ00591E
25. Doadrio JC, Sousa EMB, Izquierdo-Barba I et al (2006) Functionalization of mesoporous materials with long alkyl chains as a strategy for controlling drug delivery pattern. J Mater Chem 16:462–466. https://doi.org/10.1039/B510101H
26. Jadhav SA, Brunella V, Miletto I et al (2016) Synthesis of poly(N -isopropylacrylamide) by distillation precipitation polymerization and quantitative grafting on mesoporous silica. J Appl Polym Sci 133. https://doi.org/10.1002/app.44181
27. Khan MS, Khan GT, Khan A, Sultana S (2013) Preparation and Characterization of Novel Temperature and pH Sensitive (NIPAM-co-MAA) Polymer Microgels and Their Volume Phase Change with Various Salts. Polym Korea 37:794–801. https://doi.org/10.7317/pk.2013.37.6.794
28. Gao X, Cao Y, Song X et al (2013) pH- and thermo-responsive poly(N-isopropylacrylamide-co-acrylic acid derivative) copolymers and hydrogels with LCST dependent on pH and alkyl side groups. J Mater Chem B 1:5578. https://doi.org/10.1039/c3tb20901f
29. Qian W, Wang H, Chen J, Kong Y (2015) Spherical V-Fe-MCM-48: The Synthesis, Characterization and Hydrothermal Stability. Materials (Basel) 8:1752–1765. https://doi.org/10.3390/ma8041752
30. Qu Y, Feng L, Tong C et al (2013) Poly(p-phenylenevinylene) functionalized fluorescent mesoporous silica nanoparticles for drug release and cell imaging. Microporous Mesoporous Mater 182:155–164. https://doi.org/10.1016/j.micromeso.2013.08.045
31. Colilla M, Martínez-Carmona M, Sánchez-Salcedo S et al (2014) A novel zwitterionic bioceramic with dual antibacterial capability. J Mater Chem B 2:5639–5651. https://doi.org/10.1039/C4TB00690A

32. Kitahara Y, Okuyama K, Ozawa K et al (2012) Thermal decomposition of acrylamide from polyacrylamide. J Therm Anal Calorim 110:423–429. https://doi.org/10.1007/s10973-012-2544-7
33. Nagase K, Kobayashi J, Kikuchi A et al (2008) Effects of Graft Densities and Chain Lengths on Separation of Bioactive Compounds by Nanolayered Thermoresponsive Polymer Brush Surfaces. Langmuir 24:511–517. https://doi.org/10.1021/la701839s
34. Humphreys BA, Prescott SW, Murdoch TJ et al (2019) Influence of molecular weight on PNIPAM brush modified colloidal silica particles. Soft Matter 15:55–64. https://doi.org/10.1039/C8SM01824C
35. Sing KSW, Everett DH, Haul RAW, Moscou L, Pierotti RA, Rouquerol J, Siemieniewska T (1985) Reporting physisorption data for gas/solid systems with special reference to the determination of surface area and porosity. Pure Appl Chem 57:603–619. https://doi.org/10.1515/iupac.57.0007
36. Kullmann J, Enke D, Thraenert S et al (2010) Characterization of nanoporous monoliths using nitrogen adsorption and positronium annihilation lifetime spectroscopy. Colloids Surfaces A Physicochem Eng Asp 357:17–20. https://doi.org/10.1016/j.colsurfa.2009.09.030
37. Gidley DW, Peng H-G, Vallery RS (2006) Positron annihilation as a method to characterize porous materials. Annu Rev Mater Res 36:49–79. https://doi.org/10.1146/annurev.matsci.36.111904.135144
38. Thornton AW, Jelfs KE, Konstas K et al (2016) Porosity in metal-organic framework glasses. Chem Commun 52:3750. https://doi.org/10.1039/c5cc10072k
39. Tanis-Kanbur MB, Peinador RI, Calvo JI et al (2021) Porosimetric membrane characterization techniques: A review. J Memb Sci 619:118750. https://doi.org/10.1016/j.memsci.2020.118750
40. Schneider D, Attallah AG, Wassersleben S et al (2020) Advanced textural characterization of biogenic silica by nitrogen physisorption, positron annihilation lifetime spectroscopy and hyperpolarized 129Xe NMR spectroscopy. Microporous Mesoporous Mater 307:110515. https://doi.org/10.1016/j.micromeso.2020.110515
41. Zaleski R, Błażewicz A, Kierys A (2013) Ortho-positronium migration in mesopores of MCM-41, MSF and SBA-3. Nukleonika 58:235–240 https://www.researchgate.net/publication/280640481
42. Zaleski R, Kierys A, Dziadosz M et al (2012) Positron annihilation and N2 adsorption for nanopore determination in silica-polymer composites. RSC Adv 2:3729. https://doi.org/10.1039/c2ra20147j
43. Jadhav SA, Nisticò R, Magnacca G, Scalarone D (2018) Packed hybrid silica nanoparticles as sorbents with thermo-switchable surface chemistry and pore size for fast extraction of environmental pollutants. RSC Adv 8:1246–1254. https://doi.org/10.1039/C7RA11869D